Tunnelling between excited $^4T_2$ and ^2E states of Cr^{3+} ions with small energy separation-the case of GSGG

1989 J. Phys.: Condens. Matter 1 9175

(http://iopscience.iop.org/0953-8984/1/46/010)

J. Phys.: Condens. Matter 1 (1989) 9175–9182. Printed in the UK

Tunnelling between excited $^4T_2$ and ^2E states of Cr^{3+} ions with small energy separation—the case of GSGG

M Yamaga†, B Henderson‡ and K P O'Donnell‡

† Department of Information and Computer Science,
Toyohashi University of Technology, Toyohashi, 440, Japan

‡ Department of Physics and Applied Physics, University of Strathclyde,
Glasgow G4 0NG, UK

Received 29 September 1988, in final form 30 May 1989

Abstract. A model of $^2E \rightarrow {}^4T_2$ tunnelling induced by zero-point vibrations is developed to account for the observed temperature dependence in the photoluminescence spectrum of Cr^{3+} ions in crystals with small energy separation $\Delta E = E(^2E) - E(^4T_2)$. The model gives good agreement with experimental results for Cr^{3+}-doped $Gd_3Sc_2Ga_3O_{12}$, where $\Delta E = 70$ cm^{-1} is smaller than the mean phonon energy $\hbar\omega \simeq 180$ cm^{-1}.

1. Introduction

The $3d^3$ ion Cr^{3+} is the optical centre responsible for tunable solid state laser action at room temperature in numerous ionic crystals (Moulton 1985, Henderson and Imbusch 1988). The electronic energy levels of this ion are determined by interaction of the 3d electrons with the electrostatic field of the host and the modification of free-ion inter-electron interactions by the crystal environment (Tanabe and Sugano 1954, Sugano *et al* 1970). Whether ^2E or $^4T_2$ is the lowest excited state is determined by the strength of the octahedral crystal field. In strong crystal field sites (e.g. Al_2O_3 or MgO) the lowest excited state of Cr^{3+}, ^2E, gives rise to the R-line emission and its associated phonon side band. In weak crystal fields (e.g. $ZnWO_4$) the lowest excited state is changed to $^4T_2$. Since this state is derived from the 3d electron configuration $t_{2g}^2e_g$, where the e_g orbital points along the axes of the octahedron directly towards the ligands, the electron–phonon coupling is strong and gives rise to broad $^4A_2 \leftrightarrow {}^4T_2$ absorption and emission bands.

Systematic changes in the crystal field strength may be achieved in the garnets having the chemical formula $A_3B_2C_3O_{12}$ by variation of the crystal composition. The lattice constants of such crystals as YAG ($Y_3Al_5O_{12}$), YGG ($Y_3Ga_5O_{12}$), GGG ($Gd_3Ga_5O_{12}$), GSAG ($Gd_3Sc_2Al_3O_{12}$), GSGG ($Gd_3Sc_2Ga_3O_{12}$) and LLGG ($La_3Lu_2Ga_3O_{12}$) increase progressively along this series (Geller 1967), the change in lattice constant reflecting different distances between a central Cr^{3+} ion on the octahedral B sites and the six nearest-neighbour O^{2-} ions. It is this distance which determines the strength of the octahedral crystal field experienced by the Cr^{3+} ion. The crystal fields in YAG, YGG and GGG are strong, whereas that in LLGG is weak (Kolbe *et al* 1985, Petermann and Huber 1984). GSGG is intermediate between the two extremes, the $^4T_2$ and ^2E levels being close together in energy (Struve and Huber 1985). This paper discusses the variation of the ratio of the emission intensities from the $^4T_2$ and ^2E states with temperature in terms of phonon-assisted tunnelling between these almost degenerate states at low temperatures.

0953-8984/89/469175 + 08 $02.50

2. Theory of tunnelling between ^2E and $^4T_2$ states

2.1. Vibronic states of ^2E and $^4T_2$ levels

Transition metal ions in ionic crystals interact strongly with lattice phonons because of the spatial extent of the d electron wavefunction in the crystal. The Hamiltonian operator, including electron–phonon $H_{e\text{-}p}(r, R)$ and spin–orbit $H_{s\text{-}o}(r)$ interactions, is written as

$$H = -(\hbar^2/2M)\nabla_R^2 - (\hbar^2/2m)\nabla_r^2 + V_e(r) + V_N(R) + H_{e\text{-}p}(r, R) + H_{s\text{-}o} \tag{1}$$

where M and m are effective nuclear and electronic masses ∇_R^2 and ∇_r^2 respectively, which operate on the nuclear and electronic coordinates, and $V_E(r)$ is the electronic interaction. The harmonic potential $V_N(R)$ is given by

$$V_N(R) = \tfrac{1}{2}KR^2 = \tfrac{1}{2}M\omega^2R^2 \tag{2}$$

R being the displacement from the equilibrium ionic separation, K the vibrational force constant and ω the harmonic oscillator frequency. The electron–phonon interaction $H_{e\text{-}p}(r, R)$ consists of two terms in which the coupling coefficients are independent of and dependent on electronic (r) and nuclear (R) coordinates respectively:

$$H_{e\text{-}p}(r, R) = V_{e\text{-}p}(R) + V'_{e\text{-}p}(r, R) \qquad e = -Cr + D(r, R)R^2. \tag{3}$$

In equation (3) the higher-order terms in R are assumed to be negligible, since they are normally small compared to the linear interaction term.

We solve equation (1) for the ^2E and $^4T_2$ states of the Cr^{3+} ion in GSGG. Here, the term $V'_{e\text{-}p}(r, R)$ in equation (3) is assumed to be small compared to $V_{e\text{-}p}(R)$ and $H_{e\text{-}p}(r, R)$ tends to $-C_jR$. In the Born–Oppenheimer approximation, the vibronic wavefunction $\Psi_j(r, R)$ of the Cr^{3+} ion may be written as the product of an electronic wavefunction $\psi_j(r, R)$ and a nuclear vibrational wavefunction $\varphi_{jl}(R)$, where r and R are electronic and nuclear coordinates respectively and subscripts j and l denote different states. Equation (1) can be divided into two equations: one being associated with the electronic wavefunction and the other with the nuclear wavefunction:

$$[-(\hbar^2/2m)\nabla_r^2 + V_E(r) + \tfrac{1}{2}K_jR^2 - C_jR + H_{s\text{-}o}(r)]\psi_j(r) = e_j(R)\psi_j(r) \tag{4}$$

$$[-(\hbar^2/2M)\nabla_R^2 + e_j(R)]\varphi_{jl}(R) = E_{jl}\varphi_{jl}(R). \tag{5}$$

As the lattice relaxation energy $E_L(= C_j^2/2K)$ is fairly large compared to the spin–orbit interaction, the term $H_{s\text{-}o}(r)$ in equation (4) is regarded as a perturbation. $H_{s\text{-}o}$ admixes the wavefunctions $\chi_E(r)$ of the ^2E state and $\chi_T(r)$ of the $^4T_2$ states which are the zero-order eigenfunctions in equation (4). The secular matrix of equation (4) relative to the perturbation is

$$\begin{array}{c} \\ \chi_E(r) \\ \chi_T(r) \end{array} \begin{array}{c} \begin{array}{cc} \chi_E(r) & \chi_T(r) \end{array} \\ \begin{bmatrix} E_E(R) & \lambda \\ \lambda & E_T(R) \end{bmatrix} \end{array} \tag{6}$$

with $E_E(R)$ and $E_T(R)$ given by

$$E_E(R) = E_E(0) + \tfrac{1}{2}K_ER^2 - C_ER \qquad E_T(R) = E_T(0) + \tfrac{1}{2}K_TR^2 - C_TR \tag{7}$$

where λ is the spin–orbit splitting between ^2E and $^4T_2$ levels, and $E_E(0)$ and $E_T(0)$ are the energy levels of ^2E and $^4T_2$ at the equilibrium position ($R = 0$). The potential energies of ^2E and $^4T_2$ states are calculated numerically using equations (5), (6) and (7).

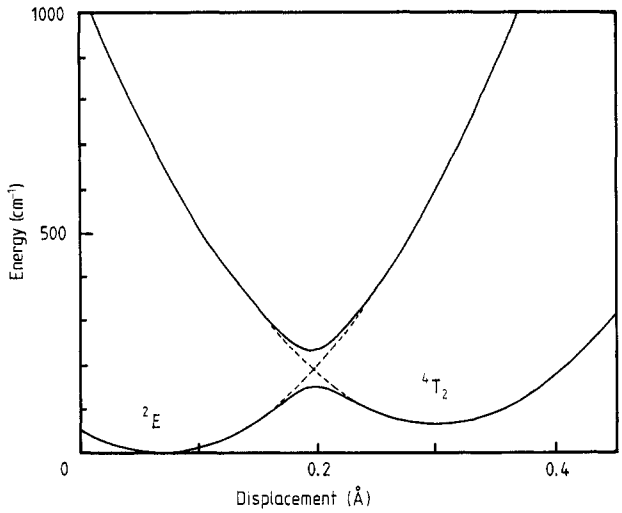

Figure 1. Potential energies of ^2E and $^4T_2$ levels admixed by spin–orbit coupling.

We now estimate the physical parameters. The Huang-Rhys factors S defined as (e.g. Henderson and Imbusch 1988)

$$S = E_L/\hbar\omega \tag{8}$$

are estimated from the shapes of the emission from the ^2E and $^4T_2$ levels to be 0.3 and 6 for the R line and broadband of GSGG respectively. The relaxation energies $E_L(E)$ and $E_L(T)$ are then estimated to be 50 cm^{-1} and 1000 cm^{-1}. The parameters $K = K_E = K_T$ $(= M\omega^2) = 30\ kg\ s^{-2}$, $C_E = (2KE_L(E))^{1/2} = 2.4 \times 10^{-10}\ kg\ m\ s^{-2}$, $C_T = (2KE_T(E))^{1/2} = 1.1 \times 10^{-9}\ kg\ m\ s^{-2}$ and $\lambda = 50\ cm^{-1}$ are determined using the relaxation energies E_L with a mean phonon energy of $\hbar\omega = 180\ cm^{-1}$ and atomic mass of oxygen $M = 2.68 \times 10^{-26}$ kg for oxygen. Figure 1 shows the potential energies $e_E(R)$ and $e_T(R)$ in equation (4) with a separation energy of 70 cm^{-1}, as a function of displacement from the equilibrium separation between the Cr^{3+} ion and its nearest-neighbour O^{2-} ions. Figure 1 also shows that the vibronic ^2E and $^4T_2$ levels are separated by a potential barrier.

The vibrational wavefunction $\varphi_{j0}(R)$ is the ground state wavefunction of a harmonic oscillator centred on the new equilibrium position determined by the linear interaction term in equation (3); it is given by

$$\Phi_{j0}(R) = (\alpha_j/\sqrt{\pi})^{1/2} \exp(-\tfrac{1}{2}\alpha_j^2(R - R_{0j})^2) \qquad (j = E, T) \tag{9}$$

where $\alpha_j^{-1} = (\hbar/M\omega)^{1/2}$ and $R_{0j} = C_j/K$. When the kinetic energy of nuclear motion is small and negligible, or when the electron is located at the bottom of the potential well, the wavefunction may be represented by a Born–Oppenheimer product of electronic and nuclear wavefunctions. The lowest total wavefunctions for ^2E and $^4T_2$ levels, including spin–orbit interaction, are respectively

$$\begin{aligned} \psi_E(r, R) &= (A\chi_E(r) + B\chi_T(r))\varphi_{E0}(R) = \psi_E(r)\varphi_{E0}(R)) \\ \psi_T(r, R) &= (-B\chi_E(r) + A\chi_T(r)\varphi_{T0}(R) = \psi_T(r)\varphi_{T0}(R) \end{aligned} \tag{10}$$

with

$$A = \{E_T(R) - E_E(R) + [(E_T(R) - E_E(R))^2 + 4\lambda^2]^{1/2}\}/2 \qquad B = -\lambda. \tag{11}$$

The transition from ^2E to the ground state, which is both parity- and spin-forbidden, becomes allowed through spin–orbit admixture of the electronic wavefunction $\Psi_T(r)$ into $\Psi_E(r)$. The line shape of the emission is determined by the nuclear wavefunction displaced to R_{0j}. The transition probabilities from the excited states $\Psi_E(r, R)$ and $\Psi_T(r, R)$ to the ground state depends on the fractions of $\Psi_T(r)$.

2.2. Tunnelling between $^4T_2$ and ^2E

As the barrier separating the states in figure 1 is lowered until it becomes comparable with the phonon energy $\hbar\omega$, the adiabatic approximation, § 2.1, becomes invalid and at low temperature tunnelling occurs between two potential minima. We then assume that the vibronic states are represented by the linear combination of localised states $\Psi_j(r)\varphi_{jl}(R)$:

$$\Psi(r, R) = \sum_{j,l} a_{jl}\psi_j(r)\varphi_{jl}(R). \tag{12}$$

Tunnelling occurs through zero-point vibrations around the equilibrium point at low temperatures. The electron–phonon interaction $V'_{e\text{-}p}(r, R)$, which is a function of electronic and nuclear coordinates, admixes the $^4T_2$ and ^2E vibronic wavefunctions. The coupling $D(r, R)$, which operates on the electronic coordinates, may be transformed to the same form as the spin–orbit interaction, which mixes the wavefunctions of $^4T_2$ and ^2E with different orbital and spin multiplicities. In consequence, the electron–phonon interaction, which is equivalent to the spin–orbit perturbation, can induce excitations over the potential barrier from the potential minima of both vibronic ^2E and $^4T_2$ states. We now estimate the tunnelling energy produced by the effective spin–orbit interaction H_{eff}. The off-diagonal matrix element between these vibronic wavefunctions of equation (10) produced by the zero-point vibrations is given by

$$\langle\psi_E(r,R)|V'_{e\text{-}p}(r,R)|\psi_T(r,R)\rangle = \langle\varphi_{E0}(R)|\varphi_{T0}(R)\rangle\langle\psi_E(r)|H_{\text{eff}}|\psi_T(r)\rangle = q\lambda'_{\text{eff}} \tag{13}$$

where

$$q = \langle\varphi_{E0}(R)|\varphi_{T0}(R)\rangle = \exp(-\tfrac{3}{2}V/\hbar\omega) \tag{14}$$

is a reduction factor for a one-dimensional vibrational mode (Ham 1965, 1968) and V is a barrier height. The secular matrix is

$$\begin{array}{c} \\ \Psi_E(r, R) \\ \Psi_T(r, R) \end{array} \begin{array}{c} \begin{array}{cc} \Psi_E(r, R) & \Psi_T(r, R) \end{array} \\ \begin{bmatrix} 0 & q\lambda'_{\text{eff}} \\ q\lambda'_{\text{eff}} & \Delta \end{bmatrix} \end{array} \tag{15}$$

where Δ is the separation energy between ^2E and $^4T_2$. The energy origin is defined as that of the unperturbed ^2E level. The eigenvalues and eigenfunctions are

$$E_E = [\Delta - (\Delta^2 + 4(q\lambda'_{\text{eff}})^2)^{1/2}]/2 \qquad \Psi'_E(r, R) = \alpha\Psi_E(r, R) + \beta\Psi_T(r, R) \tag{16a}$$

$$E_T = [\Delta + (\Delta^2 + 4(q\lambda'_{\text{eff}})^2)^{1/2}]/2 \qquad \Psi'_T(r, R) = -\beta\Psi_E(r, R) + \alpha\Psi_T(r, R) \tag{16b}$$

with

$$\alpha = \{\Delta + [\Delta^2 + 4(q\lambda'_{\text{eff}})^2]^{1/2}\}/2\Delta^2 \qquad \beta = -q\lambda'_{\text{eff}}. \tag{17}$$

Equations (16) show that at low temperatures emission from ^2E and $^4T_2$ coexist with intensity ratio proportional to $(\alpha)^2:(\beta)^2$.

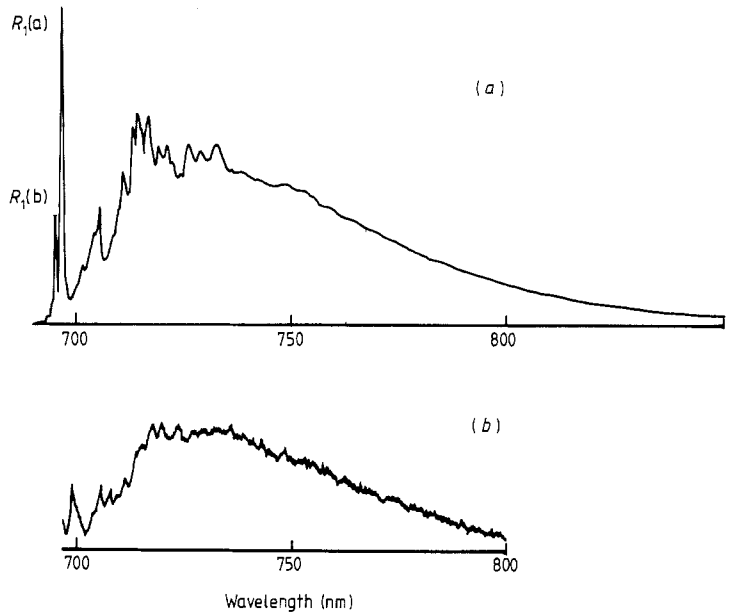

Figure 2. The photoluminescence spectrum of Cr^{3+} : GSGG measured at 4.2 K. In (*a*) the excitation wavelength is the 488 nm radiation from a Ar^+ laser, whereas (*b*) corresponds to resonant excitation at 697.5 nm in the long-wavelength tail of the R_1(a) line.

3. Comparison of experimental results with theory

The single-crystal growth of GSGG by the Czochralski technique has been described in earlier publications (Marshall 1988, Henderson *et al* 1988). Photoluminescence spectra were excited using radiation at 488 nm from an Ar^+ ion laser or tunable radiation (650–700 nm) from a ring dye laser pumped by a 3 W Ar^+ ion laser. The resulting emitted radiation was detected at right angles to the excitation direction through a 1 m grating monochromator using a GaAs phototube and a current amplifier. The sample temperature was controlled between 8–300 K or between 1.6–4.2 K using a closed-cycle cryo-refrigerator and variable temperature cryostat respectively. Earlier studies of the spectral characteristics of the emission from Cr^{3+} ions in YGG, GSGG and GSAG show that the emission line shapes are strongly influenced by compositional disorder (Struve and Huber 1985, Marshall 1988) and by crystal temperature (Henderson *et al* 1988). Disorder by non-stoichiometry results in a splitting and broadening of the R lines and their vibronic sidebands, whereas temperature influences the relative intensity of the R line process and the $^4T_2 \rightarrow {}^4A_2$ broadband emission. In YGG the Cr^{3+} ion experiences a strong octahedral crystal field, so that at low temperature (<50 K) the emission is due entirely to the R line and its vibronic sideband. As temperature is increased the R line process decreases and the broad $^4T_2 \rightarrow {}^4A_2$ band increases in intensity. That the ratio I_T/I_E did not follow an Arrhenius equation as a function of reciprocal temperature was attributed to the effects of thermal expansion of the crystal on the activation energy, effectively the difference in energies of the zero-phonon levels of the ^2E and $^4T_2$ states. Lattice expansion changes the value of this splitting by some 100 cm^{-1} between 4 K and 300 K (Henderson *et al* 1988).

The luminescence spectra of Cr^{3+}-doped YAG, YGG and GGG at low temperature are also characteristic of strong fields, the dominant effects being due to the R lines and

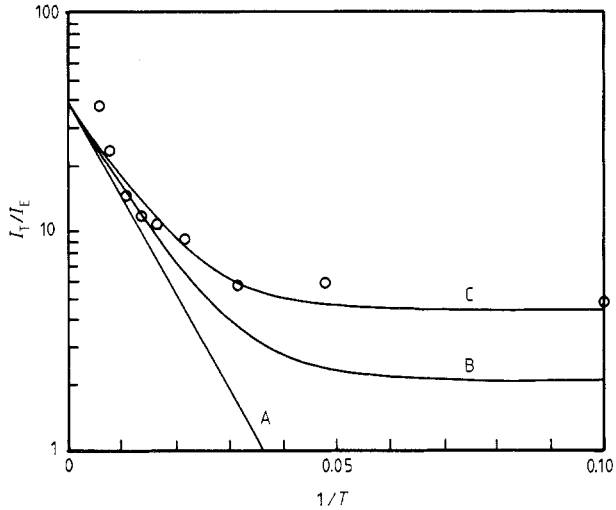

Figure 3. The intensity ratio I_T/I_E measured as a function of temperature. Full curves are calculated using equation (18) with mixing parameter ratios $(\beta)^2:(\alpha)^2$ of: A, 0:1; B, 0.05:0.95; C, 0.1:0.9.

their sidebands. The luminescence spectra from Cr^{3+} in LLGG and $ZnWO_4$ show only the broad $^4T_2 \rightarrow {}^4A_2$ band (Kolbe *et al* 1985, Petermann and Huber 1984). Figure 2 shows the emission spectra of Cr: GSGG at 4.2 K to be composed of both the broad-band and the R line and its phonon side band, whether excited with the radiation at λ = 488 nm or at 697.5 nm. The sharp lines R_1(a) and R_1(b) with wavelength λ = 696.3 nm and 694.9 nm respectively are the zero-phonon lines $^2E \rightarrow {}^4A_2$ transitions from Cr^{3+} ions at two different trigonally distorted crystal field sites (Marshall 1988). The energy separation between ^2E and $^4T_2$ is estimated to be 70 cm^{-1} from the detailed analysis of the zero-phonon lines and the phonon series of emission spectra (O'Donnell *et al* 1989). The excitation at 697.5 nm corresponds to resonant excitation in the long-wavelength tail of the R_1(a) line. The intensity of the R line and its phonon side band are weaker compared to those observed when excited at the 488 nm line, showing that the separation in energy $(E_T - E_E)$ is somewhat reduced for some Cr^{3+} ion sites. Figure 3 shows the temperature dependence of the ratio of total emission intensity of $^4T_2$ (broad band) to that of ^2E line (R line and vibronic lines). The ratio is nearly constant below 20 K and increases with an activation energy of about 70 cm^{-1} at higher temperature. Such results cannot be explained by the differing thermal populations of ^2E and $^4T_2$ states expected from a Boltzmann distribution. They may be explained by taking account of tunnelling between ^2E and $^4T_2$ states using the model developed in § 2. The calculated ratio is given by

$$\frac{I_T}{I_E} = \frac{(g_T/\tau_T)}{(g_E/\tau_E)} \frac{\beta^2 + \alpha^2 \exp(-\Delta E/kT)}{\alpha^2 + \beta^2 \exp(-\Delta E/kT)} \tag{18}$$

where $g_E(g_T)$ is the degeneracy of the state ^2E_g ($^4T_2$) and $\tau_E(\tau_T)$ is the radiative lifetime and ΔE is the energy separation between ^2E and $^4T_2$ levels tunnelling energy. The full curves A, B and C in figure 3 are calculated using equation (18) with fixed parameters $(g_T/\tau_T)/(g_E/\tau_E) = 35$, $\Delta E = 70\ cm^{-1}$. Curve A corresponds to the case of no mixing, i.e. $(\beta)^2:(\alpha)^2 = 0.0:1.0$. With admixture coefficients $(\beta)^2:(\alpha)^2 = 0.05:0.95$ and 0.1:0.9 curves B and C are obtained. The best fit is obtained using $(\beta)^2:(\alpha)^2 = 0.1:0.9$.

The mixing coefficient may also be estimated from the tunnelling splitting, $q\lambda'_{\text{eff}}$. The value of λ'_{eff} is assumed to be about 50 cm^{-1}, which is nearly equal to λ in equation (6), and the barrier height is assumed to be 200 cm^{-1} from figure 1. Then the reduction factor of 0.1 calculated using $\hbar\omega = 180\,cm^{-1}$ gives an estimated ratio $(\alpha/\beta)^2 \simeq 14$; a little larger than the observed value of 9 (Moulton 1985). This discrepancy can be explained by the disorder on the octahedral sites occupied by Cr^{3+} in this crystal. Resonant excitation at 697.5 nm (figure 2) shows that the dominant emission is from $^4T_2$, i.e. the broad band. In contrast, the broad band emission on excitation at 488 nm at 4.2 K is due to different centres on which the R_1(a) and R_1(b) lines originate, as well as from the centres creating the long-wavelength tail of the R_1(a) line (Marshall 1988, Henderson *et al* 1988). The agreement between the experimental and theoretical temperature dependence given in figure 3 is rather good, indicating that the tunnelling model is an apposite description of the emission process at low temperatures. The discrepancy at higher temperature is due in part to multi-site occupancy of Cr^{3+} ions in non-stoichiometric garnets (Struve and Huber 1985, Henderson *et al* 1988), and to the temperature dependence of ΔE which is related to the thermal expansion of the crystal. Each of the different sites occupied by the Cr^{3+} ion will have a different value of ΔE (Marshall 1988). Those with smaller ΔE, which are shown to be present by figure 2(*b*) will have an increasing effect at higher temperature, as will the reduction in ΔE by thermal expansion.

The single configurational coordinate model was applied to the excited ^2E and $^4T_2$ states of the Cr^{3+} ion by Englman and Barnett (1970), and subsequently by Fonger and Struck (1975, 1978). Tunnelling between ^2E and $^4T_2$ states of the Cr^{3+} ion was discussed by Englman and Barnett (1970), Barnett and Englman (1970). They considered both 'horizontal' and 'vertical' tunnelling. The former is tunnelling between two potential wells of the ^2E and $^4T_2$ vibronic states separated by the barrier and assisted by zero-point vibrations and optical phonons. The latter is associated with mixing of $^4T_2$ state at the same displacement coordinate into ^2E state, and corresponds to the Frank–Condon principle. Their treatment of vertical tunnelling leads to the same result as equation (10) in this paper. The transition from the ^2E state to the $^4A_2$ ground state, which is spin- and parity-forbidden, is allowed because of spin–orbit interaction (vertical tunnelling) and odd-parity distortions. The luminescence from ^2E level shows the sharp line shape because the vibronic wavefunction of $^4T_2$ vibronic state mixed into the ^2E vibronic state is the same as that of ^2E vibronic state, as is shown by equation (10). The radiative decay then depends on the mixing coefficient. On the other hand, horizontal tunnelling (tunnelling by zero-point vibration in this paper) mixes ^2E and $^4T_2$ vibronic states which have different lattice configurations. If the tunnelling probability is not too large, the eigenfunction can be represented by linear combinations of ^2E and $^4T_2$ vibronic wavefunctions without horizontal tunnelling. The luminescence spectrum at low temperatures is then an admixture of the emissions from ^2E and $^4T_2$ levels, and the ratio of the total emission intensities of $^4T_2$ and ^2E at low temperatures does not show the thermal equilibrium (Boltzmann) distribution, but tends to a constant value. Englman and Barnett (1970) also discuss tunnelling from the first and second $^4T_2$ vibronic states. Tunnelling probabilities from the second $^4T_2$ states is much larger than that from the $^4T_2$ state because the barrier height for the second $^4T_2$ state is lower than that for the first state, and the admixture of ^2E state into the second state is larger than that in the first state. This being the case, the emission of ^2E state including tunnelling process from the second $^4T_2$ state has maximal intensity at the temperature of $(\hbar\omega/2k)$.

In the potential energy curves of ^2E and $^4T_2$ states of Cr^{3+} : GSGG calculated using the parameters estimated from the low-temperature absorption and emission spectra shown in figure 1, the barrier height is estimated to be only 200 cm^{-1}, so that the bound state

in each well is only the first vibronic level. Consequently, the emission intensity of ^2E state at low temperatures does not show the steep rise discussed by Barnett and Englman (1970) but tends to a constant value as shown in figure 3. Apparently Cr^{3+} : GSGG, having small energy separation between ^2E and $^4T_2$ states, is a good example for testing the tunnelling model with different configurational coordinates.

4. Concluding remarks

The Cr^{3+} emission spectrum in garnet crystals is strongly dependent upon temperature. In YGG, where Cr^{3+} ions occupy strong crystal field sites, the temperature dependence of the ratio I_T/I_R is proportional to $\exp(-\Delta E(T)/kT)$, where $\Delta E(T)$ is large and dependent on temperature owing to the significant thermal expansion of garnets (Henderson *et al* 1988). In GSGG (and in GSAG also) emission from $^4T_2$ and ^2E states is always present even at $T < 4$ K. A model is presented here which involves tunnelling between the vibronic ^2E and $^4T_2$ levels in the presence of perturbations in the electronic wavefunctions induced by zero-point vibrations. Good agreement is obtained between experiment and theory, although such agreement could be improved by including the temperature dependence of ΔE and occupation of several sites by Cr^{3+} with different values of ΔE.

Acknowledgments

This programme of work was initiated during 1987 when M Yamaga was a Senior Visiting Fellow sponsored by SERC at the University of Strathclyde. The authors are grateful to the SERC, British Telecom Research Laboratory and the Procurement Executive, Ministry of Defence for generous support of this research work. A Marshall is thanked for his help in making some of the early measurements. The crystal used in this and the earlier studies was grown at RSRE by Dr B Cockayne and his colleagues M J Crosbie and J G Plant.

References

Barnett B and Englman R 1970 *J. Lumin.* **3** 37
Englman R and Barnett B 1970 *J. Lumin.* **3** 55
Fonger W H and Struck C W 1975 *Phys. Rev.* B **11** 3251
—— 1978 *J. Chem. Phys.* **69** 4171
Geller S 1967 *Z. Kristallogr. Suppl.* **125** 1
Ham F S 1965 *Phys. Rev.* A**138** 1727
—— 1968 *Phys. Rev.* **166** 307
Henderson B and Imbusch G F 1988 *Contemp. Phys.* **29** 235
Henderson B, Marshall A, Yamaga M, O'Donnell K P and Cockayne B 1988 *J. Phys. C: Solid State Phys.* **21** 6187
Kolbe W, Petermann K and Huber G 1985 *IEEE J. Quantum Electron.* **QE-21** 1596
Marshall A 1988 *PhD Thesis* University of Strathclyde
Moulton P M 1985 *Laser Handbook* vol 5, ed. M Bass and M L Stitch (Amsterdam: North-Holland) p 203
O'Donnell K P, Marshall A, Yamaga M, Henderson B and Cockayne B 1989 *J. Lumin.* submitted
Petermann K and Huber G 1984 *J. Lumin.* **31/32** 71
Struve B and Huber G 1985 *Appl. Phys.* B **36** 195
Sugano S, Tanabe Y and Kamimura H 1970 *Multiplets of Transition Metal Ions in Crystals* (New York: Academic)
Tanabe Y and Sugano S 1954 *J. Phys. Soc. Japan* **9** 753, 766